Coupled Thermoelasticity of a Functionally Graded Cracked layer under thermomechanical shocks

Masoud Mahdizadeh Rokhi*, Mahmoud Shariati

Department of Mechanical Engineering, Shahrood University of Technology, Shahrood, Iran

This paper investigates linear-elastic response of cracked FG layers subjected to thermomechanical loading. Classical coupled thermoelastic equations are used in the calculations. The coupled dynamical system of equations obtained from the extended finite element discretization is solved by the Newmark method in the time domain. Micromechanical models for conventional composites are used to estimate properties of FG layer. The interaction integral is then employed to calculate the stress intensity factors at each time step. Also crack propagation phenomenon under thermomechanical shocks is investigated in this paper. We have used MATLAB software to implement the algorithm and related code of problem.

Keywords: Coupled Thermoelasticity, Fracture, Crack Propagation, FGMs, Thermomechanical shocks.

1. Introduction

Functionally graded materials (FGMs) are a new class of composite materials characterized by the gradual variation in microstructure and material properties. FGMs were initially designed as thermal barrier materials for aerospace structural applications and fusion reactors. They are now developed for general use as structural components in extremely high-temperature environments. FGM components are generally constructed to sustain severe temperature gradients. Ceramic materials, because of their excellent properties at high temperatures and their superior wear and corrosion resistance, use widely in structure of FGMs. One major limitation of ceramics is their intrinsic brittleness that can result in fracture under severe thermal shocks. Therefore, the fracture analyses of FGMs under thermal shocks are important to their permanence in engineering applications.

To adapt the standard finite element method to fracture computations, the extended finite element method (XFEM) has been developed, which completely avoids remeshing [1, 2, 3]. This XFEM is based on the partition of unity [4]. In this method, a discontinuous enrichment function is used along the crack path in order to describe a discontinuous displacement [2]. Belytschko et al.

* Corresponding Author, Tel: +989153082813, Fax: +98273 3391460
Email address: masoud_mahdizadeh@yahoo.com

[5] developed a method for dynamic crack growth with loss of hyperbolicity as a propagation criterion. Rozycki et al. [6] studied the critical time step within XFEM in explicit dynamic crack propagation with enrichment kept active during the propagation. Linder and Armero [7] have treated dynamic crack propagation with embedded discontinuity elements. Menouillard et al. [8] presented a new method for crack tip enrichment based on letting the enrichment be a function of time.

The response of functionally graded cracked layers under thermomechanical shocks is found in just a few articles. Noda [9] and Fujimoto and Noda [10, 11] have done a series of works on using the finite element method to obtain the crack SIFs under thermal loading conditions in homogeneous and functionally graded materials. They considered the heat conduction equation where thermo-coupling has been ignored. Jin and Paulino [12] studied an edge crack in a strip of a functionally graded material under transient thermal loading conditions. They employed a multi-layered material model to obtain the temperature field. Without considering the thermoelastic coupling effect, transient elastodynamic crack analyses in functionally graded materials have been presented previously by many researchers in literature using various methods, see e.g. reference [13, 14] for more references cited therein. Hosseini–Tehrani and Eslami [15] and Hosseini-Tehrani et al. [16] employed the boundary element method to investigate the effect of the coupling and inertia terms in dynamical thermal loading problems. Duflot [17] investigated the static case of thermoelastic fracture by XFEM where both 2D and 3D problems with different crack face thermal boundary conditions are included. KC and Kim [18] using finite element method evaluated the non-singular T-stress and mixed-mode stress intensity factors in FGMs under steady-state thermal loads via interaction integral. Zamani and Eslami [19] employed the finite element method to obtain the SIF for a functionally graded cracked body under coupled classical thermoelastic assumption. They assumed that the crack remain stationary within simulation. Also, the XFEM formulation was implemented by Zamani and Eslami [20] to model the effect of the mechanical and thermal shocks on a cracked body. The crack was assumed to be stationary. Feng and Jin [21] examined the fracture behavior of a FGM plate containing parallel surface cracks with alternating lengths subjected to a thermal shock. Ekhlakov et al. [22] developed a boundary-domain element method (BDEM) for a transient thermoelastic crack analysis in isotropic, continuously non-homogeneous and linear elastic FGMs. They considered a stationary edge crack in a two dimensional finite domain subjected to a thermal shock and computed stress intensity factors.

The study of crack propagation phenomena in a functionally graded cracked layer under thermomechanical shocks and using the coupled thermoelastic equations is not found in previous articles. In present study, XFEM formulation is implemented to model the effect of thermal shocks on a functionally graded cracked layer under coupled classical thermoelastic assumption. The

Newmark time integration scheme is used to solve the dynamical system of matrix equations obtained from the spatial discretization of initial coupled equations. The most general form of interaction integral for FGMs is extracted base on the non-equilibrium formulation and also dynamical stress intensity factors are computed in each time step. A MATLAB code is developed to implement the different stages of computation from mesh generation to calculation of SIFs and crack propagation simulation. Some numerical examples are implemented to investigate the validity and accuracy of the written computer program. The effects of volume fraction profiles of FGMs on SIFs are investigated in this paper. The crack is assumed to be moving under thermal and mechanical shocks. Also, Crack propagation phenomenon is considered which seems not to be reported with this condition in previous works.

2. General problem formulation

2.1. Space discretization

The general governing equations of the classical coupled thermoelasticity are the equation of motion (Eq. (2-1)) and the first law of thermodynamics (Eq. (2-2)), as [23],

$$\sigma_{ij,j} + B_i = \rho \ddot{u}_i \tag{2-1}$$

$$q_{i,i} + \rho c_t \dot{\theta} + T_0(1 + \theta/T_0)\beta \dot{\varepsilon}_{ii} = R \tag{2-2}$$

If the temperature change, θ, is small compared to the reference temperature T_0, Eq. (2-2) may be approximately written in the simpler form [23].

$$q_{i,i} + \rho c_t \dot{\theta} + T_0 \beta \dot{\varepsilon}_{ii} = R \tag{2-3}$$

The system of coupled equations (2-1) and (2-2) does not have a general analytical solution. The extended finite element model of the problem is obtained by discretizing the solution domain into a number of arbitrary elements. In the XFEM formulation, a standard local displacement approximation around the crack is enriched with discontinuous jump function across the crack faces and the asymptotic crack tip displacement field around the crack tip [1]. The same procedure is used for the temperature enrichment [17]. The formulation of the XFEM for displacement components can be written as [20],

$$\begin{aligned} \mathbf{u}(x,y,t) = & \sum_{\text{all nodes}} N_n(x,y)\mathbf{a}_n(t) + \sum_{n \in N_{cr}} N_n(x,y)[H(x,y) - H(x_n,y_n)]\mathbf{b}_n(t) \\ & + \sum_{m} \sum_{n \in N_{tip}} N_n(x,y)[F_m(r,\varphi) - F_m(r_n,\varphi_n)]\mathbf{c}_{nm}(t) \end{aligned} \tag{2-4}$$

Where N_{cr} is the set of nodes that the discontinuity has in its influence domain, while N_{tip} is the set of nodes inside a predefined area around the crack tip (see fig. 1). Here, $H(x,y)$ is Heaviside enrichment function and F_m represents crack tip enrichment functions [24]. Also

$\mathbf{a}_n(t) = \{\mathrm{a}_n^{\mathrm{u}}(t), \mathrm{a}_n^{\mathrm{v}}(t)\}^{\mathrm{T}}$, $\mathbf{b}_n(t) = \{\mathrm{b}_n^{\mathrm{u}}(t), \mathrm{b}_n^{\mathrm{v}}(t)\}^{\mathrm{T}}$ and $\mathbf{c}_{nm}(t) = \{\mathrm{c}_{nm}^{\mathrm{u}}(t), \mathrm{c}_{nm}^{\mathrm{v}}(t)\}^{\mathrm{T}}$ are vectors of nodal unknowns.

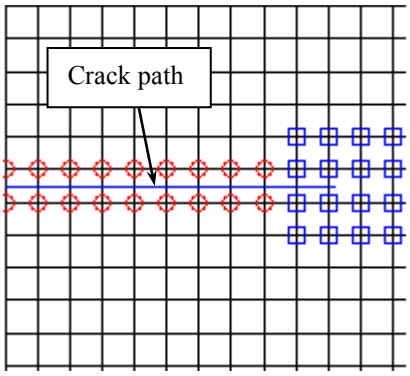

Fig. 1. Selection of enriched nodes for edge crack. Circled nodes are enriched by the discontinuity function whereas the squared nodes are enriched by the crack tip enrichment functions.

In this study the crack faces are assumed to be adiabatic so the temperature is discontinuous along the crack faces and the heat flux is singular at the crack tip. Thus, the temperature field is discretized similar to the displacement field, but only with the one crack tip enrichment function [20].

$$\boldsymbol{\theta}(x,y,t) = \sum_{all\ nodes} N_n(x,y)\mathrm{a}_n^T(t) + \sum_{n\in N_{cr}} N_n(x,y)[H(x,y) - H(x_n,y_n)]\mathrm{b}_n^T(t) + \sum_{n\in N_{tip}} N_n(\mathrm{x},\mathrm{y})[r^{0.5}\,sin(\varphi/2) - r^{0.5}\,sin(\varphi_n/2)]\mathrm{c}_n^T(t) \tag{2-5}$$

Where r and φ are the usual crack-tip polar coordinates. Also $\mathrm{a}_n^T(t)$, $\mathrm{b}_n^T(t)$ and $\mathrm{c}_n^T(t)$ are nodal unknowns corresponding to temperature field. Now, the base element (e) with n nodal points is considered and the displacement components and temperature change in the element (e) are approximated by compact forms as follows:

$$\mathbf{u}^{\mathrm{e}}(x,y,t) = N_h(x,y)\mathrm{a}_h^{\mathrm{u}}(t) + \Phi_h(x,y)\mathrm{b}_h^{\mathrm{u}}(t) + \Psi_{hm}(x,y)\mathrm{c}_{hm}^{\mathrm{u}}(t) \tag{2-6}$$

$$\mathbf{v}^{\mathrm{e}}(x,y,t) = N_h(x,y)\mathrm{a}_h^{\mathrm{v}}(t) + \Phi_h(x,y)\mathrm{b}_h^{\mathrm{v}}(t) + \Psi_{hm}(x,y)\mathrm{c}_{hm}^{\mathrm{v}}(t) \tag{2-7}$$

$$\boldsymbol{\theta}^{\mathrm{e}}(x,y,t) = N_h(x,y)\mathrm{a}_h^T(t) + \Phi_h(x,y)\mathrm{b}_h^T(t) + \Psi_{hm}(x,y)\mathrm{c}_{hm}^T(t) \tag{2-8}$$

$$h = 1,2,\dots,ne \quad m = 1,2,3,4$$

Where ne is number of nodes in element (e) and $\mathrm{c}_{nm}^T(t)$ is components of vector $\mathbf{c}^{\mathrm{T}}(t)$ defined by

$$\mathbf{c}^{\mathrm{T}}(t) = \{\mathrm{c}_{11}^T, 0,0,0, \mathrm{c}_{21}^T, 0,0,0, \mathrm{c}_{31}^T, 0,0,0, \mathrm{c}_{41}^T, 0,0,0,\} \tag{2-9}$$

Also Φ and Ψ exhibit the enriched parts of both displacement and temperature fields. They can be related to face and tip enrichment respectively.

$$\Phi_h(x,y) = N_h(x,y)[H(x,y) - H(x_h,y_h)] \tag{2-10}$$

$$\Psi_h(x,y) = N_h(x,y)\big[r^{0.5}\,sin(\varphi/2) - r_h^{0.5}\,sin(\varphi_h/2)\,, r^{0.5}\,cos(\varphi/2) - r_h^{0.5}\,cos(\varphi_h/2),$$
$$r^{0.5}\,sin(\varphi)sin(\varphi/2) - r_h^{0.5}\,sin(\varphi_h)sin(\varphi_h/2),$$
$$r^{0.5}\,sin(\varphi)cos(\varphi/2) - r_h^{0.5}\,sin(\varphi_h)\cos(\varphi_h/2)\big] \tag{2-11}$$

Applying the weighted residual integral to the equation of motion and the energy equation with respect to the weighting functions $S_l(x,y)$, the formal Galerkin approximations reduce to

$$\int_{V(e)} \big(\sigma_{ij,j} + B_i - \rho\ddot{u}_i\big) S_l dV = 0 \qquad l = 1,2,\dots,ns \tag{2-12}$$

$$\int_{V(e)} \big(q_{i,i} + \rho c_t\dot{\theta} + T_0\beta\dot{u}_{i,i} - R\big) S_l dV = 0 \quad l = 1,2,\dots,ns \tag{2-13}$$

Where ns is the number of shape function of element (e) and S_l is component of vector $\boldsymbol{S}$.

$$\boldsymbol{S} = \{N_1, N_2, N_3, N_4, \Phi_1, \Phi_2, \Phi_3, \Phi_4, \Psi_{1m}, \Psi_{2m}, \Psi_{3m}, \Psi_{4m}\} \qquad m = 1,2,3,4 \tag{2-14}$$

Hooke's law correlates the stress tensor to the displacement components and temperature change θ via Eq. (2-15).

$$\sigma_{ij} = \mu\big(u_{i,j} + u_{j,i}\big) + \big[\lambda u_{k,k} - \beta\theta\big]\delta_{ij} \tag{2-15}$$

Where $\beta = \alpha(3\lambda + 2\mu)$ and $\theta = (T - T_0)$. According to Fourier's law of heat conduction we have,

$$q_i = -k_{ij}\theta_{,j} \tag{2-16}$$

Where k_{ij} is the coefficient of thermal conduction for a general anisotropic material. By substituting Eqs. (2-6) to (2-8), (2-15) and (2-16) into Eqs. (2-12) and (2-13) and using the Gauss divergence theorem, after some manipulations, the following equations for two dimensional coupled thermoelasticity will be obtained.

$$\begin{aligned}
&\left(\int_{V(e)} \rho S_l N_h dV\right)\ddot{\mathrm{a}}_h^{\mathrm{u}} + \left(\int_{V(e)} \rho S_l \Phi_h dV\right)\ddot{\mathrm{b}}_h^{\mathrm{u}} + \left(\int_{V(e)} \rho S_l \Psi_{hm} dV\right)\ddot{\mathrm{c}}_{hm}^{\mathrm{u}} \\
&+ \left(\int_{V(e)} \big[(\lambda + 2\mu)S_{l,x}N_{h,x} + \mu S_{l,y}N_{h,y}\big]\, dV\right)\mathrm{a}_h^{\mathrm{u}} \\
&+ \left(\int_{V(e)} \big[(\lambda + 2\mu)S_{l,x}\Phi_{h,x} + \mu S_{l,y}\Phi_{h,y}\big]\, dV\right)\mathrm{b}_h^{\mathrm{u}} \\
&+ \left(\int_{V(e)} \big[(\lambda + 2\mu)S_{l,x}\Psi_{hm,x} + \mu S_{l,y}\Psi_{hm,y}\big]\, dV\right)\mathrm{c}_{hm}^{\mathrm{u}} \\
&+ \left(\int_{V(e)} \big[\lambda S_{l,x}N_{h,y} + \mu S_{l,y}N_{h,x}\big] dV\right)\mathrm{a}_h^{\mathrm{v}} + \left(\int_{V(e)} \big[\lambda S_{l,x}\Phi_{h,y} + \mu S_{l,y}\Phi_{h,x}\big] dV\right)\mathrm{b}_h^{\mathrm{v}} \\
&+ \left(\int_{V(e)} \big[\lambda S_{l,x}\Psi_{hm,y} + \mu S_{l,y}\Psi_{hm,x}\big] dV\right)\mathrm{c}_{hm}^{\mathrm{v}}
\end{aligned} \tag{2-17}$$

$$-\int_{V(e)}\beta S_{l,x}\left(N_h \mathrm{a}_h^T+\Phi_h \mathrm{b}_h^T+\Psi_{hm}\mathrm{c}_{hm}^T\right)dV=\int_{V(e)}B_x S_l dV+\int_{A(e)}t_x^n S_l dA$$

$$\left(\int_{V(e)}\rho S_l N_h dV\right)\ddot{\mathrm{a}}_h^{\mathrm{v}}+\left(\int_{V(e)}\rho S_l \Phi_h dV\right)\ddot{\mathrm{b}}_h^{\mathrm{v}}+\left(\int_{V(e)}\rho S_l \Psi_{hm} dV\right)\ddot{\mathrm{c}}_{hm}^{\mathrm{v}}$$

$$+\left(\int_{V(e)}\left[\mu S_{l,x}N_{h,y}+\lambda S_{l,y}N_{h,x}\right]dV\right)\mathrm{a}_h^{\mathrm{u}}+\left(\int_{V(e)}\left[\mu S_{l,x}\Phi_{h,y}+\lambda S_{l,y}\Phi_{h,x}\right]dV\right)\mathrm{b}_h^{\mathrm{u}}$$

$$+\left(\int_{V(e)}\left[\mu S_{l,x}\Psi_{hm,y}+\lambda S_{l,y}\Psi_{,x}\right]dV\right)\mathrm{c}_{hm}^{\mathrm{u}}$$

$$+\left(\int_{V(e)}\left[\mu S_{l,x}N_{h,x}+(\lambda+2\mu)S_{l,y}N_{h,y}\right]dV\right)\mathrm{a}_h^{\mathrm{v}}$$

$$+\left(\int_{V(e)}\left[\mu S_{l,x}\Phi_{h,x}+(\lambda+2\mu)S_{l,y}\Phi_{h,y}\right]dV\right)\mathrm{b}_h^{\mathrm{v}}$$

$$+\left(\int_{V(e)}\left[\mu S_{l,x}\Psi_{hm,x}+(\lambda+2\mu)S_{l,y}\Psi_{hm,y}\right]dV\right)\mathrm{c}_{hm}^{\mathrm{v}}$$

(2-18)

$$-\int_{V(e)}\beta S_{l,y}(N_h \mathrm{a}_h^T+\Phi_h \mathrm{b}_h^T+\Psi_{hm}\mathrm{c}_{hm}^T)dV=\int_{V(e)}B_y S_l dV+\int_{A(e)}t_y^n S_l dA$$

$$\left(\int_{V(e)}\rho c_t S_l N_h dV\right)\dot{\mathrm{a}}_h^T+\left(\int_{V(e)}\rho c_t S_l \Phi_h dV\right)\dot{\mathrm{b}}_h^T+\left(\int_{V(e)}\rho c_t S_l \Psi_{hm} dV\right)\dot{\mathrm{c}}_{hm}^T$$

$$+\left(\int_{V(e)}\left[k_x S_{l,x}N_{h,x}+k_y S_{l,y}N_{h,y}\right]dV\right)\mathrm{a}_h^T+\left(\int_{V(e)}\left[k_x S_{l,x}\Phi_{h,x}+k_y S_{l,y}\Phi_{h,y}\right]dV\right)\mathrm{b}_h^T$$

$$+\left(\int_{V(e)}\left[k_x S_{l,x}\Psi_{h1,x}+k_y S_{l,y}\Psi_{hm,y}\right]dV\right)\mathrm{c}_{hm}^T+\left(\int_{V(e)}T_0\beta S_l N_{h,x}dV\right)\dot{\mathrm{a}}_h^{\mathrm{u}}$$

(2-19)

$$+\left(\int_{V(e)}T_0\beta S_l \Phi_{h,x}dV\right)\dot{\mathrm{b}}_h^{\mathrm{u}}+\left(\int_{V(e)}T_0\beta S_l \Psi_{hm,x}dV\right)\dot{\mathrm{c}}_{hm}^{\mathrm{u}}+\left(\int_{V(e)}T_0\beta S_l N_{h,y}dV\right)\dot{\mathrm{a}}_h^{\mathrm{v}}$$

$$+\left(\int_{V(e)}T_0\beta S_l \Phi_{h,y}dV\right)\dot{\mathrm{b}}_h^{\mathrm{v}}+\left(\int_{V(e)}T_0\beta S_l \Psi_{hm,y}dV\right)\dot{\mathrm{c}}_{hm}^{\mathrm{v}}$$

$$=\int_{V(e)}RS_l dV-\int_{A(e)}(q_x n_x)S_l dA-\int_{A(e)}(q_y n_y)S_l dA$$

$$l=1,2,\ldots,ns \qquad h=1,2,\ldots,ne \qquad m=1,2,3,4$$

Where $ne=4$ for a four node element. Equations (2-17) to (2-19) are assembled into a matrix form resulting in the general finite element coupled equation given by Eq. (2-20).

(2-20)

$$[M]\{\ddot{\Delta}\}+[C]\{\dot{\Delta}\}+[K]\{\Delta\}=\{Fr\}$$

Where $[M]$, $[C]$ and $[K]$ are mass, damping, and stiffness matrices, respectively. Generally, for base element (e) which is enriched with both Heaviside and crack tip enrichment functions, these matrices can be written as follows:

(2-21) $$[M]^{(e)} = \begin{bmatrix} [M_1] & [0]_{48\times24} \\ [0]_{24\times48} & [0]_{24\times24} \end{bmatrix}$$

(2-22) $$[C]^{(e)} = \begin{bmatrix} [0]_{48\times48} & [0]_{48\times24} \\ [C_1] & [C_2] \end{bmatrix}$$

(2-23) $$[K]^{(e)} = \begin{bmatrix} [K_1] & [K_2] \\ [0]_{24\times48} & [K_3] \end{bmatrix}$$

$\{Fr\}$ is the force vector defined by:

(2-24) $$\{F\}^{(e)} = \begin{Bmatrix} \int_{V(e)} [S]^T\{Bf\}dV + \int_{A(e)} [S]^T\{Tf\}dA \\ \int_{V(e)} R[St]^T dV - \int_{A(e)} \left(q_x n_x + q_y n_y\right)[St]^T dA \end{Bmatrix}$$

And $\{\Delta\}$ is the nodal displacements and temperature changes vector,

(2-25) $$\{\Delta\}^{(e)} = \{\mathrm{a}_h^{\mathrm{u}}, \mathrm{a}_h^{\mathrm{v}}, \mathrm{b}_h^{\mathrm{u}}, \mathrm{b}_h^{\mathrm{v}}, \mathrm{c}_{hm}^{\mathrm{u}}, \mathrm{c}_{hm}^{\mathrm{v}}, \mathrm{a}_h^T, \mathrm{b}_h^T, \mathrm{c}_{hm}^T\}^{\mathrm{T}}, \qquad h, m = 1, \dots, 4$$

Also $\{\dot{\Delta}\}$ and $\{\ddot{\Delta}\}$ are the first and second time derivative of $\{\Delta\}$, respectively. Components of mass, damping, and stiffness matrices are obtained as follows:

(2-26) $$[M_1] = \int_{V(e)} \rho[S]^{\mathrm{T}}[S]dV$$

(2-27) $$[C_1] = \int_{V(e)} T_0\beta[St]^{\mathrm{T}}[S_1]dV,$$

(2-28) $$[C_2] = \int_{V(e)} \rho c_t[St]^{\mathrm{T}}[St]dV$$

(2-29) $$[K_1] = \int_{V(e)} [S_2]^{\mathrm{T}}[D][S_2]\, dV$$

(2-30) $$[K_2] = -\int_{V(e)} \beta[S_1]^{\mathrm{T}}[St]\, dV$$

For isotropic materials $k_x = k_y = k$, therefore $[K_3]$ is obtained as follows:

(2-31) $$[K_3] = \int_{V(e)} k[S_3]^{\mathrm{T}}[S_3]dV$$

Matrices $[St]$, [S], $[S_1]$, $[S_2]$, $[S_3]$ and vectors $\{Bf\}$ and $\{Tf\}$ are derived as follows:

(2-32) $$[St] = [N_1 \quad \cdots \quad N_4 \quad \Phi_1 \quad \cdots \quad \Phi_4 \quad \Psi_{11} \quad \Psi_{21} \quad \Psi_{31} \quad \Psi_{41}]$$

$$[S] = \begin{bmatrix} N_1 & \cdots & N_4 & 0 & \cdots & \mathbf{0} & \Phi_1 & \cdots & \Phi_4 & 0 & \cdots & 0 & \Psi_{11} & \cdots & \Psi_{44} & 0 & \cdots & 0 \\ 0 & \cdots & 0 & N_1 & \cdots & N_4 & 0 & \cdots & 0 & \Phi_1 & \cdots & \Phi_4 & 0 & \cdots & 0 & \Psi_{11} & \cdots & \Psi_{44} \end{bmatrix} \tag{2-33}$$

$$[S_1] = \begin{bmatrix} N_{1,x} & \cdots & N_{4,x} & N_{1,y} & \cdots & N_{4,y} & \Phi_{1,x} & \cdots & \Phi_{4,x} & \Phi_{1,y} & \cdots & \Phi_{4,y} \\ & & & & & & \Psi_{11,x} & \cdots & \Psi_{44,x} & \Psi_{11,y} & \cdots & \Psi_{44,y} \end{bmatrix} \tag{2-34}$$

$$[S_2] = \begin{bmatrix} N_{1,x} & \cdots & N_{4,x} & 0 & \cdots & 0 & \Phi_{1,x} & \cdots & \Phi_{4,x} & 0 & \cdots & 0 & \Psi_{11,x} & \cdots & \Psi_{44,x} & 0 & \cdots & 0 \\ 0 & \cdots & 0 & N_{1,y} & \cdots & N_{4,y} & 0 & \cdots & 0 & \Phi_{1,y} & \cdots & \Phi_{4,y} & 0 & \cdots & 0 & \Psi_{11,y} & \cdots & \Psi_{44,y} \\ N_{1,y} & \cdots & N_{4,y} & N_{1,x} & \cdots & N_{4,x} & \Phi_{1,y} & \cdots & \Phi_{4,y} & \Phi_{1,x} & \cdots & \Phi_{4,x} & \Psi_{11,y} & \cdots & \Psi_{44,y} & \Psi_{11,x} & \cdots & \Psi_{44,x} \end{bmatrix} \tag{2-35}$$

$$[S_3] = \begin{bmatrix} N_{1,x} & N_{2,x} & N_{3,x} & N_{4,x} & \Phi_{1,x} & \Phi_{2,x} & \Phi_{3,x} & \Phi_{4,x} & \Psi_{11,x} & \cdots & \Psi_{44,x} \\ N_{1,y} & N_{2,y} & N_{3,y} & N_{4,y} & \Phi_{1,y} & \Phi_{2,y} & \Phi_{3,y} & \Phi_{4,y} & \Psi_{11,y} & \cdots & \Psi_{44,y} \end{bmatrix} \tag{2-36}$$

$$\{Bf\} = \begin{Bmatrix} B_x \\ B_y \end{Bmatrix}, \quad \{Tf\} = \begin{Bmatrix} t_x^n \\ t_y^n \end{Bmatrix} \tag{2-37}$$

For plane strain state matrix $[D]$ is defined as follows:

$$[D] = \frac{E}{(1+\nu)(1-2\nu)} \begin{bmatrix} 1-\nu & \nu & 0 \\ \upsilon & 1-\nu & 0 \\ 0 & 0 & (1-2\nu)/2 \end{bmatrix} \tag{2-38}$$

2.2. Time integration

Maybe the most widely used family of direct methods for solving semi discrete equation of motion is the Newmark family which consists of the following equations [25]:

$$[M]\{\ddot{\Delta}_{n+1}\} + [C]\{\dot{\Delta}_{n+1}\} + [K]\{\Delta_{n+1}\} = \{Fr_{n+1}\} \tag{2-39}$$

$$\{\Delta_{n+1}\} = \{\Delta_n\} + \Delta t\{\dot{\Delta}_{n+1}\} + \Delta t^2(1/2 - \zeta)\{\ddot{\Delta}_n\} + \Delta t^2\zeta\{\ddot{\Delta}_{n+1}\} \tag{2-40}$$

$$\{\dot{\Delta}_{n+1}\} = \{\dot{\Delta}_n\} + \Delta t(1-\gamma)\{\ddot{\Delta}_n\} + \Delta t\gamma\{\ddot{\Delta}_{n+1}\} \tag{2-41}$$

The Newmark family contains many well-known and wide used methods. The average acceleration method is one of them for structural dynamics applications which is unconditionally stable. In this method, γ and ζ are equal to $1/2$ and $1/4$ respectively. We will choose the mean acceleration scheme, which is unconditionally stable, since for the partition of unity method with an explicit Newmark-type scheme, the stable time step of the enriched problem is a small fraction of the stable time step of the problem with no enriched shape function [26].

3. Interaction integral and SIF computations

In this section, the interaction integral is formulated by superimposing the actual and auxiliary fields on the path independent J-integral [27]. In this work, the non-equilibrium formulation [28] is used in conjunction with XFEM to determine M-integral for arbitrarily oriented cracks in FGMs under thermomechanical loading and also computation of SIFs is explained in conjunction with the M-integral.

Now, we consider two independent admissible fields which are the actual ($\boldsymbol{u}$, ε, σ) and auxiliary ($\boldsymbol{u}^{aux}$, ε^{aux}, σ^{aux}) fields. The J -integral of the superimposed fields (actual and auxiliary) can be written as follows:

$$\begin{aligned} J^s = \int_{A^*} \{ & \big[\big(\sigma_{ij} + \sigma_{ij}^{aux}\big)\big(u_{j,1} + u_{j,1}^{aux}\big) - 1/2\,\big(\sigma_{jk} + \sigma_{jk}^{aux}\big)\big(\varepsilon_{jk}^{m} + \varepsilon_{jk}^{aux}\big)\delta_{1i} \\ & - 1/2\,\rho(\dot{u}_k + \dot{u}_k^{aux})(\dot{u}_k + \dot{u}_k^{aux})\delta_{1i}\big]\mathrm{q}_{,i} \\ & + \big[\big(\sigma_{ij,i} + \sigma_{ij,i}^{aux}\big)\big(u_{j,1} + u_{j,1}^{aux}\big) + \big(\sigma_{ij} + \sigma_{ij}^{aux}\big)\big(u_{j,1i} + u_{j,1i}^{aux}\big) \\ & - 1/2\,\big(\sigma_{ij} + \sigma_{ij}^{aux}\big)\big(\varepsilon_{ij,1}^{m} + \varepsilon_{ij,1}^{aux}\big) - 1/2\,\big(\sigma_{ij,1} + \sigma_{ij,1}^{aux}\big)\big(\varepsilon_{ij}^{m} + \varepsilon_{ij}^{aux}\big) \\ & - \rho(\dot{u}_i + \dot{u}_i^{aux})\big(\dot{u}_{i,1} + \dot{u}_{i,1}^{aux}\big) - 1/2\,\rho_{,1}(\dot{u}_i + \dot{u}_i^{aux})(\dot{u}_i + \dot{u}_i^{aux})\big]\mathrm{q}\big\}dA \end{aligned} \tag{3-1}$$

Where q is a weight function varying from unity at the crack tip to zero on boundary of domain A^* [28]. Eq. (3-1) is decomposed into

$$J^s = J + J^{aux} + MI \tag{3-2}$$

Where J and J^{aux} are given respectively by Eqs. (3-3) and (3-4).

$$\begin{aligned} J = \int_{A^*} \{ & \big[\sigma_{ij}u_{j,1} - 1/2\,\sigma_{jk}\varepsilon_{jk}^{m}\delta_{1i} - 1/2\,\rho\dot{u}_k\dot{u}_k\delta_{1i}\big]\mathrm{q}_{,i} \\ & + \big[\sigma_{ij,i}u_{j,1} + \sigma_{ij}u_{j,1i} - 1/2\,\sigma_{ij}\varepsilon_{ij,1}^{m} - 1/2\,\sigma_{ij,1}\varepsilon_{ij}^{m} - \rho\dot{u}_i\dot{u}_{i,1} - 1/2\,\rho_{,1}\dot{u}_i\dot{u}_i\big]\mathrm{q}\big\}dA \end{aligned} \tag{3-3}$$

$$\begin{aligned} J^{aux} = \int_{A^*} \{ & \big[\sigma_{ij}^{aux}u_{j,1}^{aux} - 1/2\,\sigma_{jk}^{aux}\varepsilon_{jk}^{aux}\delta_{1i} - 1/2\,\rho\dot{u}_k^{aux}\dot{u}_k^{aux}\delta_{1i}\big]\mathrm{q}_{,i} \\ & + \big[\sigma_{ij,i}^{aux}u_{j,1}^{aux} + \sigma_{ij}^{aux}u_{j,1i}^{aux} - 1/2\,\sigma_{ij}^{aux}\varepsilon_{ij,1}^{aux} - 1/2\,\sigma_{ij,1}^{aux}\varepsilon_{ij}^{aux} - \rho\dot{u}_i^{aux}\dot{u}_{i,1}^{aux} \\ & - 1/2\,\rho_{,1}\dot{u}_i^{aux}\dot{u}_i^{aux}\big]\mathrm{q}\big\}dA \end{aligned} \tag{3-4}$$

The resulting M-integral is given by

$$\begin{aligned} MI = \int_{A^*} \{ & \big[\sigma_{ij}u_{j,1}^{aux} + \sigma_{ij}^{aux}u_{j,1} - 1/2\,\sigma_{jk}\varepsilon_{jk}^{aux}\delta_{1i} - 1/2\,\sigma_{jk}^{aux}\varepsilon_{jk}^{m}\delta_{1i} - \rho\dot{u}_k\dot{u}_k^{aux}\delta_{1i}\big]\mathrm{q}_{,i} \\ & + \big[\sigma_{ij,i}u_{j,1}^{aux} + \sigma_{ij,i}^{aux}u_{j,1} + \sigma_{ij}u_{j,1i}^{aux} + \sigma_{ij}^{aux}u_{j,1i} - 1/2\,\sigma_{ij}\varepsilon_{ij,1}^{aux} \\ & - 1/2\,\sigma_{ij}^{aux}\varepsilon_{ij,1}^{m} - 1/2\,\sigma_{ij,1}\varepsilon_{ij}^{aux} - 1/2\,\sigma_{ij,1}^{aux}\varepsilon_{ij}^{m} - \rho\dot{u}_i\dot{u}_{i,1}^{aux} - \rho\dot{u}_i^{aux}\dot{u}_{i,1} \\ & - \rho_{,1}\dot{u}_i\dot{u}_i^{aux}\big]\mathrm{q}\big\}dA \end{aligned} \tag{3-5}$$

Since the actual fields employ the quantities obtained from numerical simulation, the equilibrium and compatibility condition are satisfied. For the auxiliary fields, the equilibrium condition is not satisfied [28], i.e., $\sigma_{ij,i}^{aux} \neq 0$. While the relation between strain and displacement is compatible, i.e., $\varepsilon_{ij}^{aux} = 0.5\left(u_{i,j}^{aux} + u_{j,i}^{aux}\right)$ and $\sigma_{ij}u_{j,1i}^{aux} = \sigma_{ij}\varepsilon_{ij,1}^{aux}$. The auxiliary stress field is defined as follows:

$$\sigma_{ij}^{aux} = C_{ijkl}(x)\varepsilon_{ij}^{aux} \tag{3-6}$$

Notice that the auxiliary fields are chosen as asymptotic fields for homogeneous materials. Auxiliary fields, used in this paper, are based on Williams' solution [29] for stationary cracks and Swenson and Ingraffea [30] for moving cracks. The resulting interaction integral (MI) becomes

$$\begin{aligned} MI = \int_{A^*} \{ & \left[\sigma_{ij}u_{j,1}^{aux} + \sigma_{ij}^{aux}u_{j,1} - \sigma_{jk}\varepsilon_{jk}^{aux}\delta_{1i} - \rho\dot{u}_k\dot{u}_k^{aux}\delta_{1i}\right]\mathrm{q}_{,i} \\ & + \left[\rho\ddot{u}_j u_{j,1}^{aux} + \sigma_{ij,i}^{aux}u_{j,1} + \sigma_{ij}^{aux}\left(\alpha_{,1}\theta + \alpha\theta_{,1}\right)\delta_{ij} - \left(C_{ijkl,1}\varepsilon_{kl}^{m}\varepsilon_{ij}^{aux}\right)\right. \\ & \left. - \rho\dot{u}_i\dot{u}_{i,1}^{aux} - \rho\dot{u}_i^{aux}\dot{u}_{i,1} - \rho_{,1}\dot{u}_i\dot{u}_i^{aux}\right]\mathrm{q}\}dA \end{aligned} \tag{3-7}$$

Since the Numerical computation of displacements, strains, stresses, etc., is based on the global coordinate system, first the M-integral is evaluated in the global (MI_{global}) and then transformed into the local coordinate system (MI_{local}). The global M-integral quantities are evaluated by

$$\begin{aligned} (MI_n)_{global} = \int_{A^*} & \left\{\left[\sigma_{ij}u_{j,n}^{aux} + \sigma_{ij}^{aux}u_{j,n} - \sigma_{jk}\varepsilon_{jk}^{aux}\delta_{ni} - \rho\dot{u}_k\dot{u}_k^{aux}\delta_{ni}\right]\frac{\partial \mathrm{q}}{\partial X_i}\right. \\ & + \left[\rho\ddot{u}_j u_{j,n}^{aux} + \sigma_{ij,i}^{aux}u_{j,n} + \sigma_{ij}^{aux}\left(\alpha_{,n}\theta + \alpha\theta_{,n}\right)\delta_{ij} - \left(C_{ijkl,n}\varepsilon_{kl}^{m}\varepsilon_{ij}^{aux}\right)\right. \\ & \left.\left. - \rho\dot{u}_i\dot{u}_{i,n}^{aux} - \rho\dot{u}_i^{aux}\dot{u}_{i,n} - \rho_{,n}\dot{u}_i\dot{u}_i^{aux}\right]\mathrm{q}\right\}dA \quad n = 1,2 \end{aligned} \tag{3-8}$$

Where X_i denotes the global coordinate system. The local M-integral quantity is given as [28].

$$MI_{local} = (MI_1)_{global}cos\omega + (MI_2)_{global}sin\omega \tag{3-9}$$

Where ω is the angle between local and global Cartesian coordinate systems on crack tip. The relation between M-integral and SIFs for stationary crack in plane strain state is as follows:

$$MI_{local} = 2\left(1 - \nu_{tip}^2\right)\left(K_I K_I^{aux} + K_{II}K_{II}^{aux}\right)/E_{tip} \tag{3-10}$$

Also, for moving crack MI_{local} can be obtained from Eq. (3-11) [8].

$$MI_{local} = 2\left(1 - \nu_{tip}^2\right)\left[\beta_1(\dot{a})K_I K_I^{aux} + \beta_2(\dot{a})K_{II}K_{II}^{aux}\right]/E_{tip} \tag{3-11}$$

Where E_{tip} and ν_{tip} denote Young's modulus and Poisson's ratio at crack tip respectively and $\dot{a}$ is crack velocity. β_i are the universal functions (see [8]). Consequently, K_I and K_{II} are calculated by choosing $K_I^{aux} = 1$, $K_{II}^{aux} = 0$ and $K_I^{aux} = 0$, $K_{II}^{aux} = 1$, respectively. The equivalent dynamic stress intensity factor K^{eq} is defined by Eq. (3-12) [8]:

(3-12) $$K^{eq} = K_I cos^3(\omega_c/2) - 1.5K_{II} cos(\omega_c/2) sin\omega_c$$

Where ω_c is the direction in which the crack will propagate from its current tip, and will be obtained using the maximum hoop stress criteria [8].

(3-13) $$\omega_c = 2\arctan(0.25[K_I/K_{II} - sign(K_{II})((K_I/K_{II})^2 + 8)^{0.5}]), \quad -\pi < \omega_c < \pi$$

In dynamic fracture mechanics, the initiation of growth and continued propagation of a crack depend on the equivalent stress intensity factor K^{eq} relative to the material critical stress intensity factor, K_{IC}. While $K^{eq} < K_{IC}$, the crack tip remains stationary. If $K^{eq} \geq K_{IC}$ the crack tip will be move. In this paper, we use an algorithm similar to algorithm presented in reference [26] to detect crack propagation phenomenon.

4. Modeling of functionally graded layer

The material properties of the functionally graded layer must be described across the layer thickness. In the present analysis, we assume that the material gradation is along the *x* direction and the volume fraction of inclusion follows a simple power function,

(4-1) $$V_i(x) = (x/L)^{\mathrm{p}}$$

Where V_i is the volume fraction of inclusion and p is the power exponent determining the volume fraction profiles.

We assume that the functionally graded layer is made of metal-phase and ceramic-phase. In this study, we use micromechanical models for conventional composites given by Hatta and Taya [31] and Mori and Tanaka [32] to calculate the properties of functionally graded ceramics (FGCs). Also, the fracture toughness of the two-phase FGC composite needs to be determined. Here we adopt Jin and Batra's rule of mixtures formula for a two phase FGC composite [33].

(4-2) $$K_{IC}(x) = \{V_1(x)(K_{IC}^1)^2 + V_2(x)(K_{IC}^2)^2\}^{1/2}$$

To incorporate these relations into the XFE model, first the value of each material property is calculated at each individual node based on micromechanical models. Then, material properties at each Gaussian integration point can be interpolated from the nodal material properties of the element using isoparametric shape functions which are the same for spatial coordinates (*x*, *y*). Thus, material properties such as elastic modulus (E), Poisson's ratio (ν), and mass density (ρ) at Gauss points can be interpolated using shape functions from nodal points as [34]

(4-3) $$E = \sum_{i=1}^{m} N_i E_i, \qquad \nu = \sum_{i=1}^{m} N_i \nu_i, \qquad \rho = \sum_{i=1}^{m} N_i \rho_i$$

5. Numerical examples

In This section, first we present tree numerical examples which examine the accuracy and precision of presented method in this paper. Then we consider the effect of volume fraction profile of FGMs and loading condition on crack tip SIFs in next example. In the last example, we study the crack propagation phenomenon in a FG layer under thermal and mechanical shocks. The plane strain state is assumed in all numerical examples.

5.1. First example

We consider an elastic two dimensional isotropic and homogeneous layer with an edge crack (fig. 2). The initial temperature T_0 is chosen to be 400°K. The layer is rapidly cooled by conduction at its left surface to T_1, which is equal to 350°K in this study. All other sides are assumed to be thermally insulated. In this example, we neglect the coupling term in the energy equation as Lee and Sim [35] did in their analytical solution and the attained SIFs are compared with their analytical solution.

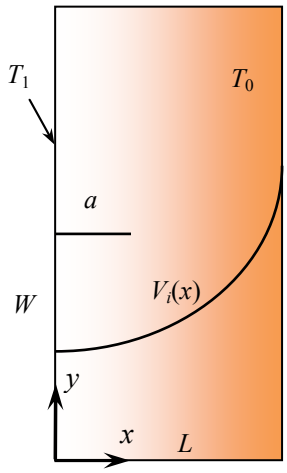

Fig. 2. Geometry and boundary condition of layer.

The problem dimensions are L = 0.001m, W = 0.002m and a = 0.00005m (fig. 2). The material properties are ρ = 5600 kg/m3, E = 117 GPa, ν = 0.333, α = 7.118×10^{-6} K^{-1}, c_t = 615.6 J/kgK and k = 2.036 W/mK. A 51× 101 four node rectangular element mesh is used and the selected time step is Δt = 10^{-4} s. A domain of 0.0001m×0.0001m was used to calculate the interaction integral and SIF. The Analytical and numerical dimensionless SIF (K_{ID}) is plotted versus the logarithm of dimensionless time (t_D) in Fig. 3, where good accordance is observed. In this example we define K_{ID} and t_D which follow from Eqs. (5-1) and (5-2) [35].

(5-1) $$K_{ID} = K_I(1-\nu)/\{E\alpha(T_0 - T_1)L^{0.5}\}$$

(5-2) $$t_D = kt/\rho c_t L^2$$

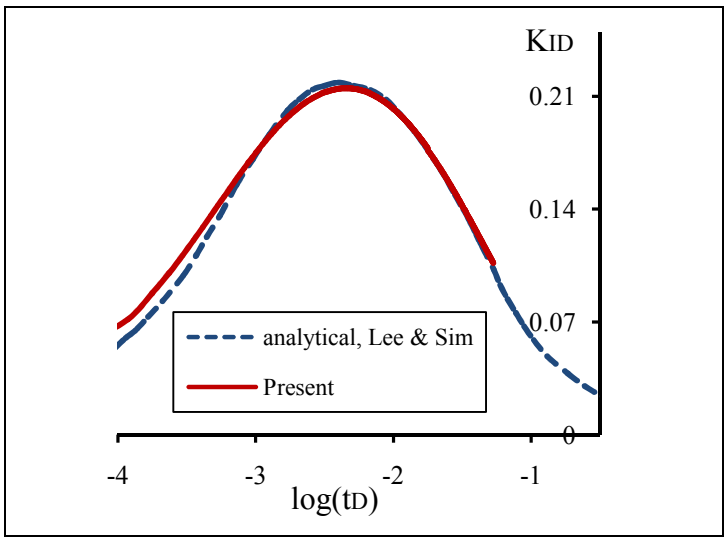

Fig. 3. Normalized SIF versus logarithm of Normalized time for first numerical example.

5.2. Second example

An FG two-dimensional layer with a horizontal edge crack is considered, as shown in Fig. 2. The layer is initially at a constant temperature. Without loss of generality, the initial temperature can be assumed to be 200°K. The layer is suddenly cooled down by conduction at its left surface to temperature T_1, which is equal to 190°K. the initial and boundary conditions for the temperature field are:

(5-3) $$T = 200^{\circ}K \quad at \ t = 0, \qquad T = 190^{\circ}K \quad at \ x = 0, \qquad T = 200^{\circ}K \quad at \ x = L$$

We suppose that the heat transfer coefficient on the surfaces of the FGM strip is infinite which is an idealized thermal shock boundary condition. The problem dimensions are L = 0.001m and W = 0.002m (fig. 2). Two crack lengths are considered in this example, a = 0.0001m and a = 0.0003m. The mesh consists of 61 × 121 four node rectangular element in this example and the selected time step is Δt =2×10^{-4} s. A square domain with dimensions $2a\times2a$ was used to calculate the interaction integral and SIF.

Table 1 lists the properties of the constituent materials, i.e., Al_2O_3 and Si_3N_4. This study assumes that the volume fraction of Si_3N_4 (phase i) follows a simple power function (Eq. (4-1)). The material gradation in the x direction is considered.

Table 1. Material properties of Al_2O_3 and Si_3N_4 [21].

	Young's modulus (GPa)	Poisson's ratio	CTE (10^{-6}/K)	Thermal conductivity (W/m-K)	Mass density (Kg/m^3)	Specific heat (J/Kg-K)	Fracture toughness (MPa-m$^{1/2}$)
Al_2O_3	320	0.25	8	20	3800	900	4
Si_3N_4	320	0.25	3	35	3200	700	5

The SIFs for this two dimensional thermoelasticity problem are compared with those obtained by Jin and Paulino [12] in fig. 4 which shows a good agreement between both results. Fig. 4 illustrate that under thermal shock, increasing crack length will decrease SIF. The dimensionless thermal stress intensity factor at the crack tip and dimensionless time can be computed as follows [12]:

(5-4) $$K_{ID} = K_I(1-\nu)/\{E\alpha_0(T_0 - T_1)(\pi L)^{0.5}\}$$

(5-5) $$t_D = k_0 t/\rho_0 c_{t0} L^2$$

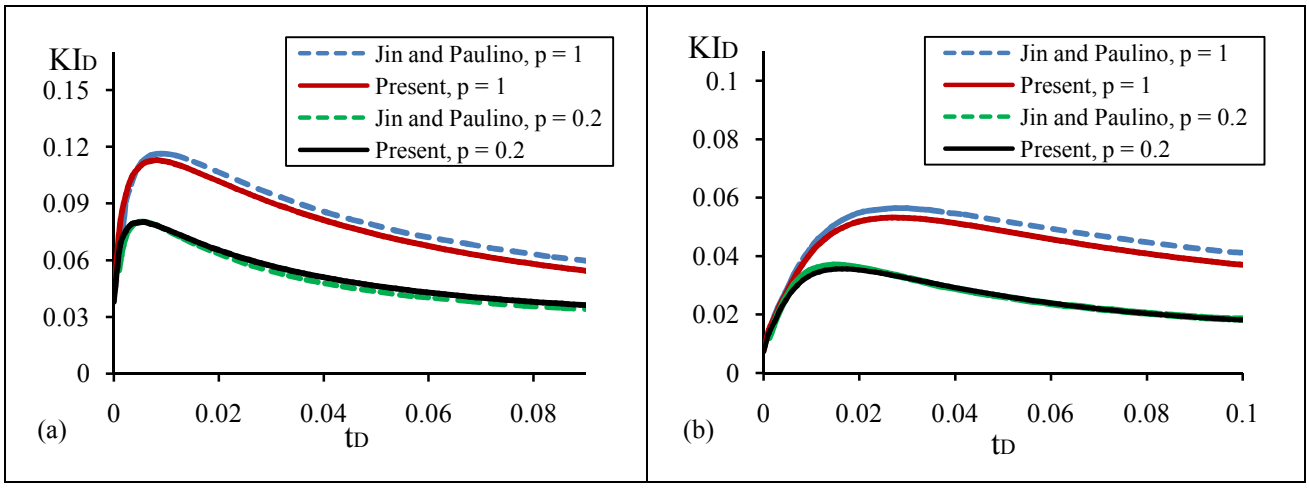

Fig. 4. Normalized SIF versus Normalized time for second numerical example, a) a/L = 0.1, b) a/L =0.3.

5.3. Third example

An elastic two-dimensional layer with an edge crack is considered in this example. A schematic of the problem is shown in Fig. 5. A uniform traction of magnitude $\sigma_0 = 63750$ Pa is applied at time $t = 0$ as a step function to the top and bottom edges. The layer dimensions are 10m×4m, and the initial crack length is a = 5m. The analytical solution given by Freund [36] is for an infinite layer. Since the specimen is finite, we stopped the simulation before the reflected wave from the edge reaches the crack tip at $t = 0.001\,s$. The material properties are $\rho = 7833\text{kg/m}^3$, $E = 200\text{GPa}$ and $\nu = 0.3$. A 201×81 quadrilateral mesh was used.

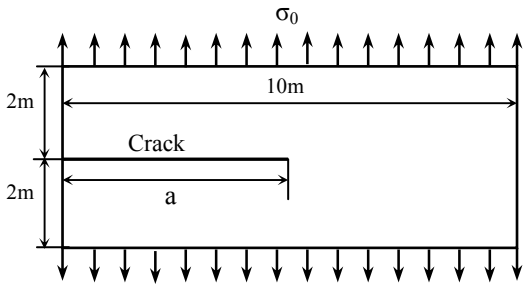

Fig. 5. Internally isotropic cracked layer under mechanical shock.

We use a domain of 0.5m×0.5m to calculate the interaction integral and SIF. The SIF values for this problem are obtained and compared with the analytical solution in fig. 6, which shows a good agreement between both results. The results are quite smooth and oscillate about the analytic solution. These unavoidable oscillations are also observed in references [37], [5], [38], [19] and [20] for the standard XFEM. These oscillations are the characteristic of the solution of a shock propagation problem by the FE discretization in the spatial domain and also by the Newmark method in the time domain [20].

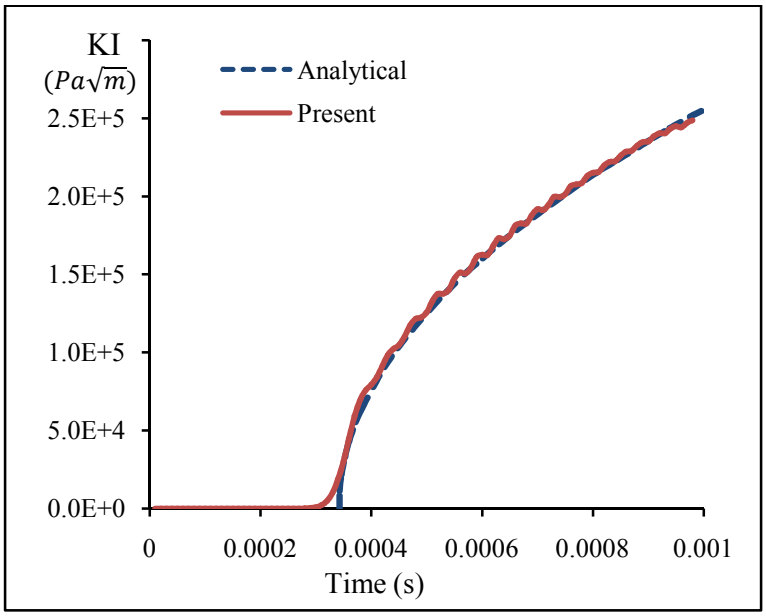

Fig. 6. Comparison variations of numerical and analytical SIF with time for the third numerical example.

5.4. Fourth Example

An elastic two-dimensional FG layer with an edge crack (Fig. 7) is considered in this example. A tension of magnitude $\sigma_0 = 10$ MPa and cooling thermal shocks of magnitude $\theta = -10$ and $\theta = -20$ is applied at time $t = 0$ as a step function to the top and bottom edges. The layer dimensions are L = 0.1m and W = 0.02m, and the initial crack length is a = 0.05m. The calculations are carried out to the point $t = 10\mu s$, before the reflected wave from the edge reaches the crack tip. Initial temperature T_0 is chosen to be 300°K.

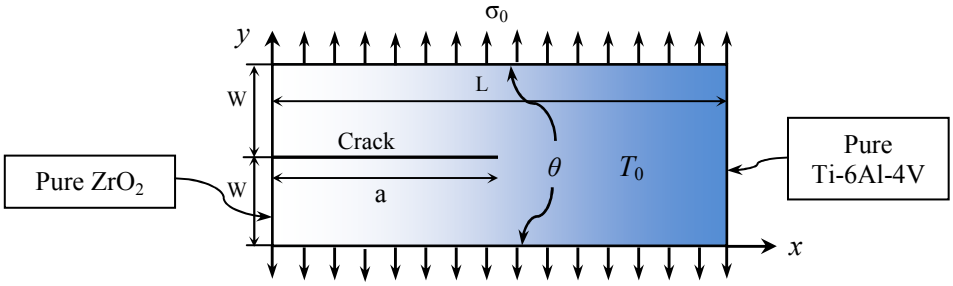

Fig. 7. Internally FG cracked layer under mechanical shock.

In these numerical calculations, we consider a Ti-6Al-4V and ZrO_2 FGM. The properties of the constituent materials are presented in table 2. The material gradation in the *x* direction is considered and the volume fraction of ZrO_2 follows than Eq. (4-1). A mesh with 81× 201 four node rectangular element is used and the selected time step is Δt =10^{-7} s. A domain of dimensions 0.005m×0.005m was used to calculate the SIF.

Table 2. Material properties of Ti-6Al-4V and ZrO_2 [20]

	Young's modulus (GPa)	Poisson's ratio	CTE (10^{-6}/K)	Thermal conductivity (W/m-K)	Mass density (Kg/m^3)	Specific heat (J/Kg-K)	Fracture toughness (MPa-m$^{1/2}$)
Ti-6Al-4V	66.2	0.321	10.3	18.1	4410	808.3	60
ZrO_2	117	0.333	7.11	2.036	5600	615.6	4

To study the effect of the material gradation, the coupled thermoelasticity problem with tree different values of *p* is analyzed (i.e. p = 0.2, p = 1 and p = 5). The time variations of the mode-I thermal dynamic SIF are shown in Fig. 8. Figures 8(a) and 8(b) demonstrate that SIF due to thermomechanical shocks is superposition of SIFs produced with thermal and mechanical shocks separately. Also figs. 8(c) and 8(d) show that increasing the material gradient parameter, p, will increase SIF regardless of loading conditions. We can see from fig. 8 that the curve related to thermal shocks is smoother than other curves.

5.5. Fifth Example

In this example, we study crack propagation phenomenon in a FG layer with a horizontal edge crack under thermal and mechanical shocks. Dimensions, properties, mesh and boundary conditions of considered layer are identical to the previous example. Initial temperature T_0 is chosen to be 500°K. A cooling thermal shock equal to -100 degree (θ = -100) and a mechanical shock of magnitude $\sigma_0 = 200$ MPa are applied to upper and bottom surface of layer. The total simulation time is $60\mu s$.

The crack tip propagation velocity for FG layers with p = 0.2 and p = 5 under thermomechanical shocks is illustrated in fig. 9. It is obtained from fig. 9 that crack propagation initiation time is dependent to loading condition and volume fraction profile of FG layer.

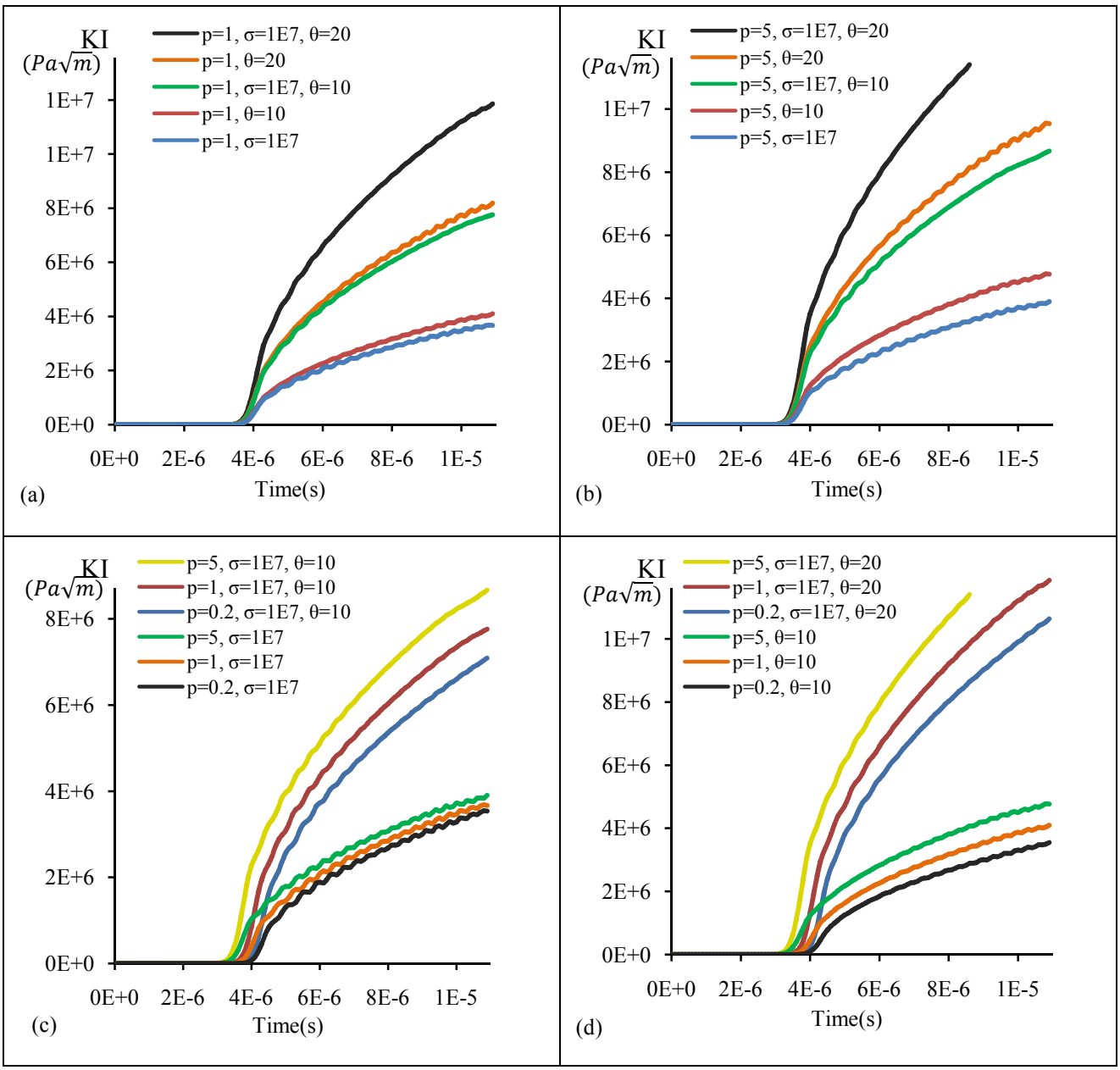

Fig. 8. Stress intensity factor versus time for the fourth numerical example in various loading conditions. a) p = 1, b) p = 5, c) mechanical and thermomechanical shock, d) thermal and thermomechanical shock.

Crack growth initiation under mechanical shocks happens earlier than crack growth initiation under thermal shocks. Also increasing material gradient parameter, p, will decrease crack propagation initiation time and will increasing crack propagation velocity. Figure 9 shows that the velocity curve related to p = 5 almost lie over curve related to p = 0.2.

Figures 10 and 11 illustrate crack propagation path, von Mises stress contours and deformed mesh for FG layers with p = 0.2 and p = 5 respectively, under thermomechanical shocks at times 10μs, 20μs and 60μs. For more clarification, displacements are multiplied by 5 in plotting deformed

meshes. Figures 10 and 11 show that crack propagates in straight line until about t = 40μs, regardless of loading conditions and material gradient parameter (p). After this time crack deviates to upward. Belytschko et al. [5] for homogeneous materials predicted that after crack propagation in straight line, crack branching may be occur but our written code doesn't have ability to detect crack branching phenomenon. Comparison of figs. 10 and 11 confirms that increasing p, will increase crack propagation velocity and crack length. Also deviation of crack path will increase with increasing p.

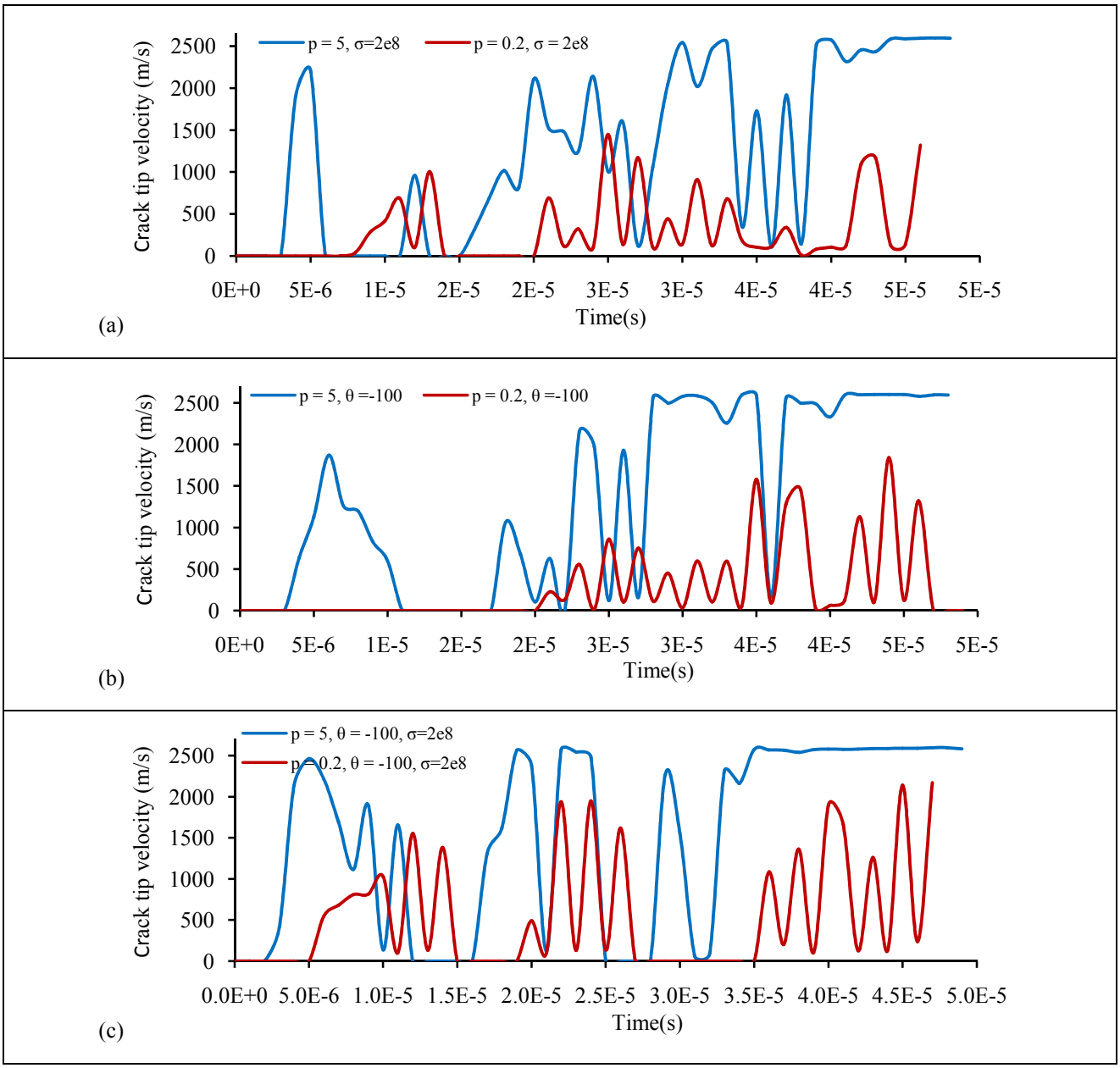

Fig. 9. Crack tip velocity for FG layers under a) Mechanical shock, b) Thermal shock, c) Thermomechanical shock.

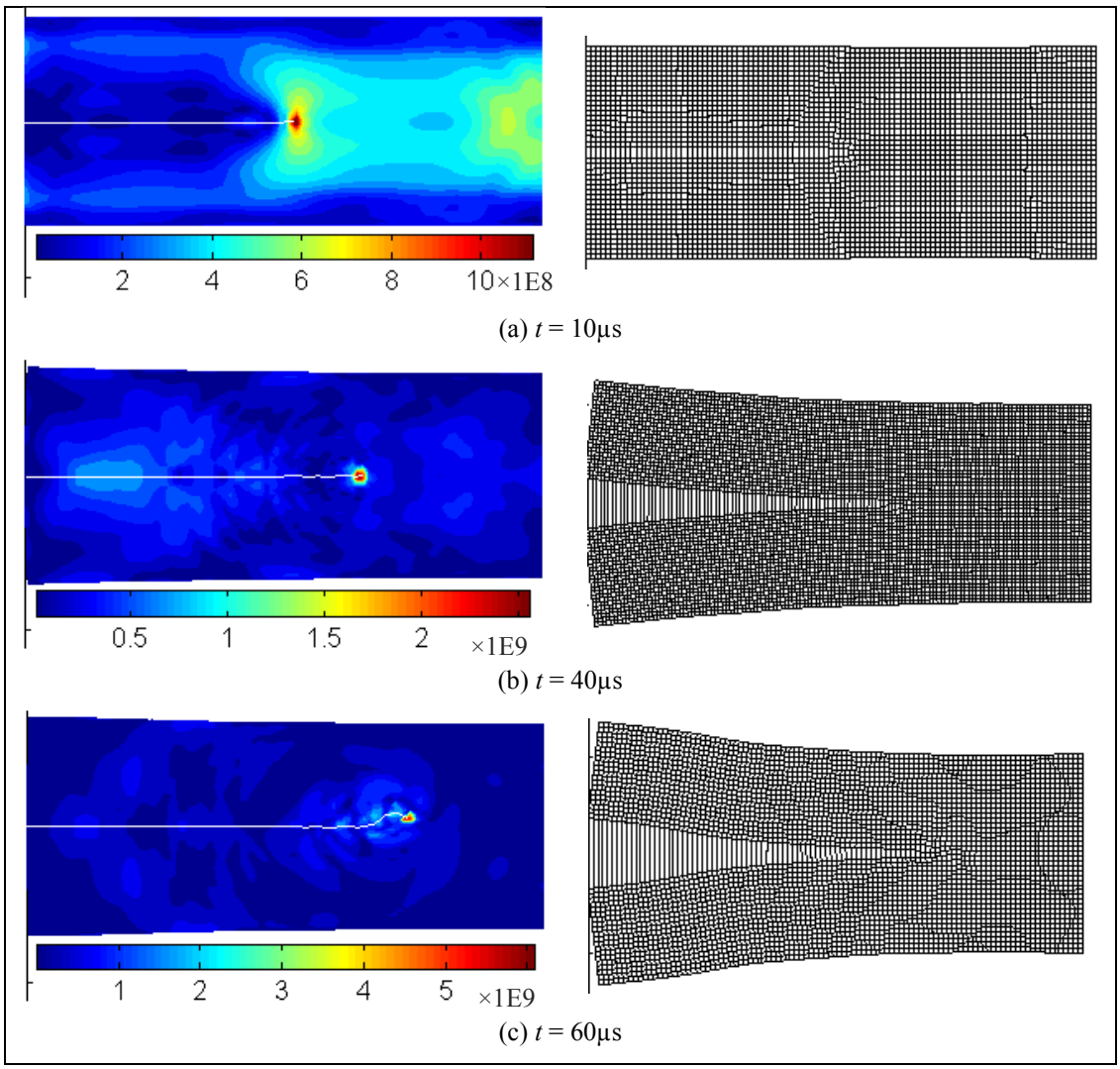

Fig. 10. Von Mises stress contours and Deformed mesh of FG layer with p =0.2 under thermomechanical shock at various times. Displacements in deformed mesh became 5 times larger for more clarification.

6. Conclusions

In this study, Classical coupled thermoelastic equations were solved using XFE and Newmark Methods in FGMs. The most general form of Interaction Integral were developed to evaluate Dynamical SIFs for both homogenous and FG materials. Also, the crack propagation phenomenon is considered in FG layers under thermomechanical shock. Some numerical examples are implemented and good agreements and accuracies are observed. The following results were obtained for a FG layer composed of Ti-6Al-4V and ZrO_2 where the crack is placed in ZrO_2 enriched side:

1- Under thermomachanical shocks in mode I, increasing the material gradient parameter, p, in a FG Layer will increase SIF (KI).

2- Crack growth initiation under mechanical shocks happens earlier than crack growth initiation under thermal shocks in mode I.

3- Increasing material gradient parameter (p), will decrease crack propagation initiation time.

4- Under thermomechanical shocks in mode I, increasing the material gradient parameter (p), will increase crack propagation velocity.

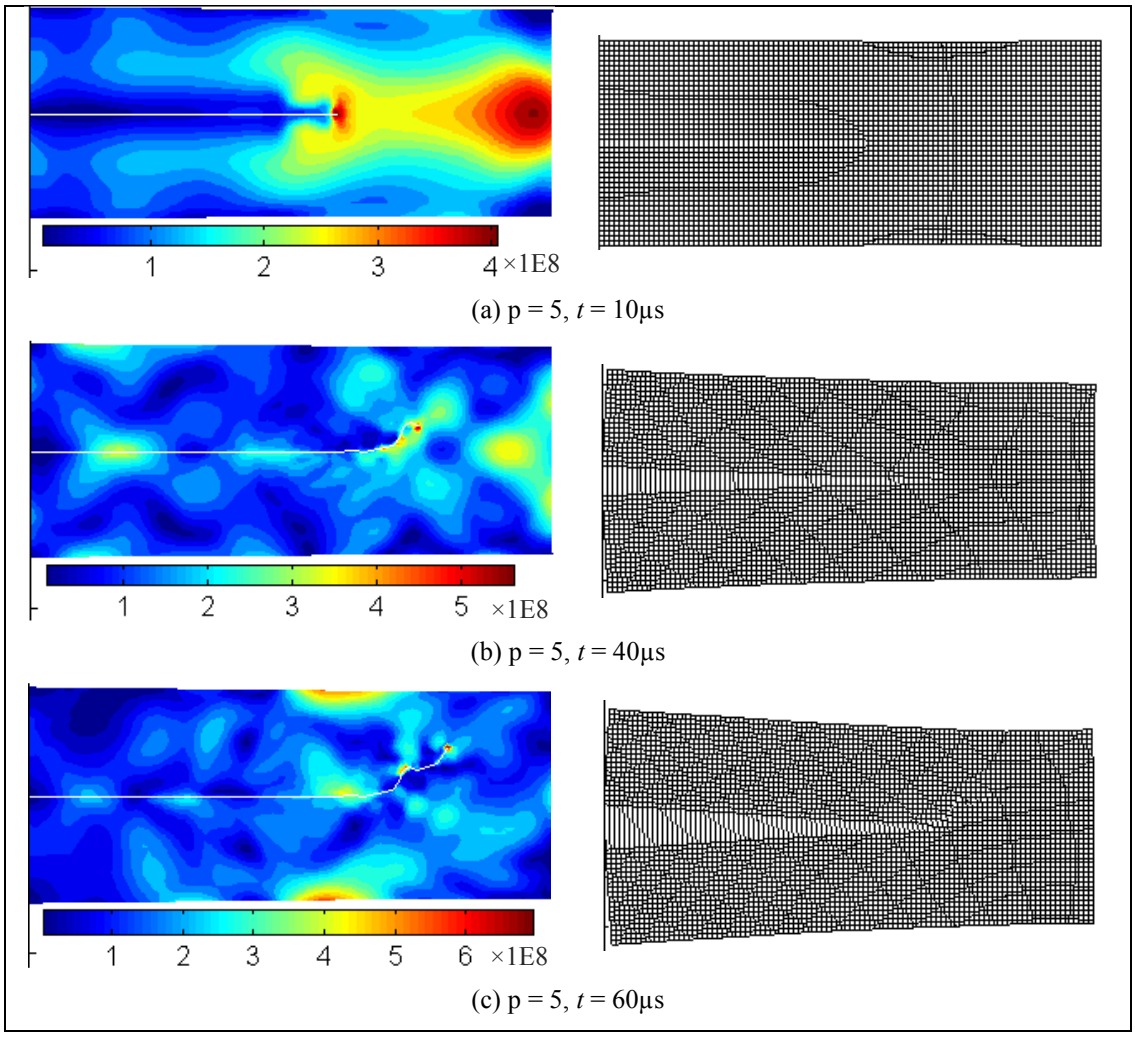

Fig. 11. Von Mises stress contours and Deformed mesh of FG layer with p =5 under thermomechanical shock at various times. Displacements in deformed mesh became 5 times larger for more clarification.

References

1. T. Black, T. Belytschko, Elastic *crack growth in finite elements with minimal remeshing*, Int. J. Numer. Method Engin., **45**, 601–620, 1999

2. N. Moës, J. Dolbow, T. Belytschko, *A finite element method for crack growth without remeshing*, Int. J. Numer. Method Engin., **46**, 1, 131–150, 1999.

3. T. Belytschko, N. Moës, S. Usui, C. Parimi, *Arbitrary discontinuities in finite elements*, Int. J. Numer. Method Engin., **50**, 4, 993–1013, 2001.

4. J. M. Melenk, I. Babuška, *The partition of unity finite element method: basic theory and applications*, Comput. Method Appl. Mech. Engin., **139**, 1–4, 289–314, 1996.

5. T. Belytschko, H. Chen, J. Xu, G. Zi, *Dynamic crack propagation based on loss of hyperbolicity and a new discontinuous enrichment*. Int. J. for Num. Method in Engin. **58**, 1873–1905, 2003.

6. P. Rozycki, N. Moës, E. Béchet, C. Dubois, *X-FEM explicit dynamics for constant strain elements to alleviate mesh constraints on internal or external boundaries*, Comput. Method Appl. Mech. Engin., **197**, 5, 349–363, 2008.

7. C. Linder, F. Armero, *Finite elements with embedded branching*. Finite Elem Anal Des, **45**, 280–293, 2009.

8. T. Menouillard, J-H. Song, Q. Duan, T. Belytschko, *Time dependent crack tip enrichment for dynamic crack propagation*, Int. J. Fract., **162**, 33–49, 2010.

9. N. Noda, *Thermal stress intensity factor for functionally gradient plate with an edge crack*, J. Therm. Stresses, **20**, 3–4, 373–387, 1997.

10. T. Fujimoto, N. Noda, *Crack propagation in a functionally graded plate under thermal shock*, Arch. Appl. Mech., **70**, 6, 377–386, 2000.

11. T. Fujimoto, N. Noda, *Two crack growths in a functionally graded plate under thermal shock*, J. Therm. Stresses, **24**, 847–862, 2001.

12. Z-H. Jin, G. H. Paulino, *Transient thermal stress analysis of an edge crack in a functionally graded material*, Int. J. Fract., **107**, 73–98, 2001.

13. Ch. Zhang, J. Sladek, V. Sladek, *Effects of Material Gradients on Transient Dynamic Mode-III Stress Intensity Factors*. International Journal of Solids and Structures, **40**, 5251-5270, 2003.

14. H. M. Xu, X. F. Yao, X. O. Feng, H.-Y. Yeh, *Dynamic stress intensity factors of a semi-infinite crack in an orthotropic functionally graded material*, Mechanics of Materials, **40**, 1, 37-47, 2008.

15. P. Hosseini-Tehrani, M. R. Eslami, H. R. Daghyani, *Dynamic crack analysis under coupled thermoelastic assumption*, J. Appl. Mech., **68**, 4, 584–588, 2001.

16. P. Hosseini-Tehrani, A. R. Hosseini-Godarzi, M. Tavangar, *Boundary element analysis of stress intensity factor KI in some two dimensional dynamic thermoelastic problems*, Eng. Anal. B. E., **29**, 232–240, 2005.

17. M. Duflot, *The extended finite element method in thermoelastic fracture mechanics*, Int. J. Num. Meth. Engin., **74**, 827–847, 2008.

18. A. KC, J-H. Kim, *Interaction integrals for thermal fracture of functionally graded materials*, Engin. Fract. Mech., **75**, 2542–2565, 2008.

19. A. Zamani, M. R. Eslami, *Coupled dynamical thermoelasticity of a functionally graded cracked layer*, J. Therm. Stresses, **32**, 969–985, 2009.

20. A. Zamani, M. R. Eslami, *Implementation of the extended finite element method for dynamic thermoelastic fracture initiation*, Int. J. Solid Struc., **47**, 1392–1404, 2010.

21. Y. Feng, Z. Jin, *Thermal fracture of functionally graded plate with parallel surface cracks*, Acta Mechanica Solida Sinica, **22**, 5, 453-464, 2009.

22. A. V. Ekhlakov, O. M. Khay, Ch. Zhang, J. Sladek, V. Sladek, *A BDEM for transient thermoelastic crack problems in functionally graded materials under thermal shock*, Comp. Mater. Scie., **57**, 30–37, 2012.

23. R. B. Hetnarski, M. R. Eslami, *Thermal Stresses – Advanced Theory and Applications*, Springer, 2009.

24. S. Mohammadi, *Extended Finite Element Method*, Blackwell Publishing Ltd, 2008.

25. T. JR. Hughes, *The finite element method*, Englewood Cliffs, New Jersey, Prentice-Hall INC. 1987.

26. C. A. Gerlach, *Computational methods for the dynamic response of cracked specimens*, Ph.D Thesis, Northwestern university, Evanston, Illinois, 1999.

27. J. R. Rice, *A path-independent integral and the approximate analysis of strain concentration by notches and cracks*, ASME J. Appl. Mech., **35**, 2, 379–386, 1968.

28. S. H. Song, G. H. Paulino, *Dynamic stress intensity factors for homogeneous and smoothly heterogeneous materials using the interaction integral method*, Int. J. Solid Struc., **43**, 4830–4866, 2006.

29. M. L. Williams, *On the stress distribution at the base of a stationary crack*, ASME J. Appl. Mech., **24**, 1, 109–114, 1957.

30. D.V. Swenson, A. R. Ingraffea, *Modeling mixed-mode dynamic crack propagation using finite elements: theory and applications*, comp. mech., **3**, 381-397, 1988.

31. H. Hatta, M. Taya, *Equivalent inclusion method for steady state heat conduction in composites*, Int. J. Engin. Scie., **24**, 520-524, 1986.

32. T. Mori, K. Tanaka, *Average stress in matrix and average elastic energy of materials with misfitting inclusions*, Acta Materialia, **21**, 571-574, 1973.

33. Z-H. Jin, R. C. Batra, Some basic fracture mechanics concepts in functionally graded materials, J. Mech. Phys. Solid, **44**, 1221-1235, 1996.

34. J-H. Kim, G. H. Paulino, *Isoparametric graded finite elements for nonhomogeneous isotropic and orthotropic materials*, ASME J. Appl. Mech., **69**, 502–514, 2002.

35. K.Y. Lee, K. B. Sim, *Thermal shock stress intensity factor by Bueckner's weight function method*, Engin. Frac. Mech., **37**, 4, 799–804, 1990.

36. L. B. Freund, *Dynamic Fracture Mechanics*, Cambridge University Press, Cambridge, 1990.

37. C. A. Duarte, O. N. Hamzeh, T. J. Liszka, W. W. Tworzydlo, *A generalized finite element method for the simulation of three dimensional dynamic crack propagation*. Computer Methods in Applied Mechanics and Engineering, **190**, 2227–2262, 2001.

38. J. Réthoré, A. Gravouil, A. Combescure, *An energy-conserving scheme for dynamic crack growth using extended finite element method*, Int. J. for Num. Methods in Engin., **63**, 631–659, 2005.